Journal of ELECTRONIC MATERIALS, Vol. 48, No. 10, 2019
https://doi.org/10.1007/s11664-019-07425-x
© 2019 The Minerals, Metals & Materials Society

Investigation of AlGaN-Based Near-Ultraviolet Light-Emitting Diodes with a Trapezoidal Electron Blocking Layer

JIHANG LI,[1] HUAIMIN GU,[1,2] GUANG LI,[1] LANG CHEN,[1] HENGZHI SHI,[1] XINGGANG SHEN,[1] XIANQI YANG,[1] NANA LIU,[1] RUI YUAN,[1] and JINYUAN ZHANG[1]

1.—Laboratory of Nanophotonic Functional Material and Devices, Institute of Opto-Electronic Materials and Technology, South China Normal University, Guangzhou 510631, China. 2.—e-mail: guhm139@139.com

To improve performance of AlGaN-based ultraviolet light-emitting diodes (UV-LEDs), an LED with a special trapezoidal electron blocking layer (EBL) is investigated numerically. The results show the optimized structure has better photoelectric performance than conventional structure. The light output power of the new structure was enhanced by a factor of 26% compared with the reference conventional LED. The reasons for these improvements are that the special trapezoidal EBL can increase the hole injection efficiency and suppress electron overflow, thus enhancing the radiative recombination rate. Consequently the light output power and the internal quantum efficiency are improved.

Key words: AlGaN-based ultraviolet light-emitting diodes, trapezoidal electron blocking layer, light output power, internal quantum efficiency

INTRODUCTION

With the continuous maturation of blue LED technology, the high Al content AlGaN-based UV-LEDs have attracted the attention of researchers due to their diverse potential applications in fields of air and water purification, solid-state white lighting, high-density optical storage, UV curing and medical photo therapy.[1–3] Although the UV-LEDs have made some impressive progress, they cannot be commercialized yet as extensively as visible LEDs. The main reason is that the IQE of the UV-LEDs is far less than that of visible LEDs. In addition, the UV-LEDs also face the problem of efficiency droop that the IQE of UV-LEDs decreases with current injection at high current. There are many factors leading to the low IQE and the severe efficiency droop, such as the poor crystalline quality of AlGaN, the Mg-doping problem in high Al content AlGaN, electron leakage, and the strong piezoelectric polarization and spontaneous polarization in multiple quantum wells (MQWs).[4–6] For the mentioned issues above, several methods have been applied to improve the performance of UV-LEDs. Including the use of AlN buffer layer to achieve high quality AlGaN epitaxial layer on Si(111) substrates,[7] the adoption of polarization doping to obtain high *p*-type AlGaN materials,[8] the design of special EBL to reduce electronic leakage,[9] and the proposal of special quantum well structure to improve the polarization effect in the active region.[10] In UV-LEDs, it is important to reduce the electron leakage because electrons have a small effective mass and high mobility, which can easily overflow across quantum barriers and EBL potential. Additionally, the hole injection efficiency is poor, due to its low mobility and inhomogeneous distribution in QWs. These factors eventually lead to low radiation recombination rates and IQE. Although the high Al content EBL plays a significant role in limiting the electrons, it also hinders the hole injection, so the content of Al can't be especially

(Received June 27, 2018; accepted July 3, 2019; published online July 11, 2019)

high. To improve the performance of UV-LEDs, the LED with a trapezoidal EBL is designed and the effect of the trapezoidal EBL is studied in this paper. It indicates that the values of light output power and the IQE of LED with trapezoidal EBL are improved, compared with conventional LED with stationary Al component EBL. These improvements are due to the enhancement of hole injection efficiency and the suppression of electron overflow.

STRUCTURE AND PARAMETERS

The structure of AlGaN based MQWs UV-LED with a conventional AlGaN EBL (denoted as original LED) is used as a reference in this study. The reference and the modified structures were grown on *c*-plane sapphire substrates. The first structure (labeled as original LED) consisted of a 3-μm-thick Si-doped n-$Al_{0.15}Ga_{0.85}N$ layer (2×10^{18} cm^{-3}), the active region including five periods of undoped GaN (3 nm)/$Al_{0.15}Ga_{0.85}N$ (10 nm) QWs, then a 20-nm-thick Mg-doped p-$Al_{0.3}Ga_{0.7}N$ EBL layer (1×10^{17} cm^{-3}) followed by a Mg-doped 90-nm-thick p-$Al_{0.15}Ga_{0.85}N$ layer (2×10^{17} cm^{-3}) and a Mg-doped 10-nm-thick p-GaN cap layer (2×10^{18} cm^{-3}). The device geometry is 300 μm × 300 μm. To improve the performance, two UV-LED structures with trapezoidal EBL are proposed. The two structures (labeled as sample A and sample B) are similar to the original LED except for the EBL, and the schematic diagrams are shown in Fig. 1. For sample A, the EBL is 3 nm $Al_xGa_{1-x}N$/14 nm $Al_{0.3}Ga_{0.7}N$/3 nm $Al_yGa_{1-y}N$, the value x increases from 0.15 to 0.3 in the growth direction, and y decreases from 0.3 to 0.15 along the vertical direction. The EBL of sample B consists of two 3 nm $Al_xGa_{1-x}N$/2.66 nm $Al_{0.3}Ga_{0.7}N$/3 nm $Al_yGa_{1-y}N$, which are separated by 2.66 nm $Al_{0.15}Ga_{0.85}N$, x and y are the same as sample A.

In this simulation, the Advanced Physical Models of Semiconductor Devices (APSYS) simulator (developed by Crosslight Software Inc) is used to analyze the optical and electrical properties of the above structures. It includes many advanced physical models such as hot carrier transport, heterojunction models, and thermal analysis. The light output power, band diagram, carrier concentration and the electronic current density of these structures can be obtained by solving Poisson's equation, the Schrödinger equation, carrier transport equations and the current continuity equation self-consistently with proper boundary conditions.[11,12] The basic physical models are described as follows:

$$\nabla \cdot J_n - \sum_j R_n^{tj} - R_{sp} - R_{st} - R_{au} + G_{opt}(t) = \frac{\partial_n}{\partial_t} + N_D \frac{\partial_{f_D}}{\partial_t}, \quad (1)$$

$$\nabla \cdot J_p + \sum_j R_p^{tj} + R_{sp} + R_{st} + R_{au} - G_{opt}(t) = \frac{\partial_p}{\partial_t} + N_A \frac{\partial_{f_A}}{\partial_t}, \quad (2)$$

$$-\nabla \cdot \left(\frac{\varepsilon_0 \varepsilon_{dc}}{q} \nabla V\right) = -n + p + N_D(1 - f_D) - N_A f_A + \sum_j N_{tj}(\delta_j - f_{tj}), \quad (3)$$

where $J_n = n\mu_n \nabla E_{fn}$ and $J_p = p\mu_p \nabla E_{fp}$ denote the densities of electrons and holes; μ_n and μ_p denote the electron mobility and hole mobility; E_{fn} and E_{fp} denote the quasi-Fermi levels of electron and hole; R_p^{tj}, R_{sp}, R_{st}, R_{au}, and $G_{opt}(t)$ denote the jth SRH deep level trap recombination rate, spontaneous radiative recombination rate, stimulated radiative recombination rate, Auger recombination rate, and light generation rate, respectively; f_D and f_A are the probabilities of electrons occupying donor and hole acceptor impurity; ∇V is the electric field; ε_{dc} is the relative dielectric constant; n and p are the electron

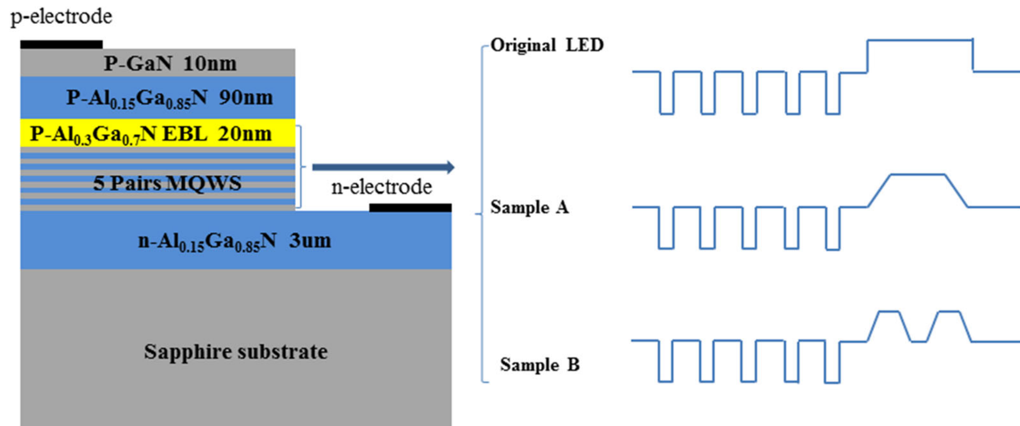

Fig. 1. The schematic diagrams of the three ultraviolet light-emitting diodes.

and hole concentration, respectively; N_A is the shallow donor doping concentration; N_D is the acceptor doping concentration; N_{tj} is the jth SRH density of deep level traps; f_{tj} is the probability of electrons occupying the jth deep level trap; and $\delta = 1$ means donor and $\delta = 0$ means acceptor. The operating temperature is set at 300 K, the Shockley–Read–Hall recombination lifetime was assumed to be 5.0 ns and internal absorption of the LED device is assumed to be 1000 m^{-1} here.[13] The Auger recombination coefficient is set to be 1×10^{-30} cm^6/s. The band-offset ratio, which is defined as the ratio between the conduction band offset ΔEc and the valence band offset ΔEv, of UV-LED is assumed to be 0.7/0.3, and the band-offset ratio ΔEc/ΔEv is serving as a default parameter in the simulation.[14] The built-in interface polarization charges due to the spontaneous and piezoelectric polarization were calculated based on the methods proposed by Fiorentini et al.[15] and scaled down by a fit factor of 0.4 accounting for the partial compensation of them by fixed defects. In order to consider the built-in polarization within the interface, the spontaneous polarization of $Al_xGa_{1-x}N$ alloys can be expressed as:

$$P_{sp}(Al_xGa_{1-x}N) = -0.090x - 0.034(1-x) + 0.019x(1-x), \quad (4)$$

On the other hand, the piezoelectric polarization of $Al_xGa_{1-x}N$ can be calculated from the following expression:

$$P_{pz}(Al_xGa_{1-x}N) = P_{pz}(AlN)x + P_{pz}(GaN)(1-x), \quad (5)$$

where

$$P_{pz}(AlN) = -1.808\varepsilon + 5.624\varepsilon^2 \quad \text{for } \varepsilon < 0, \quad (6)$$

$$P_{pz}(AlN) = -1.808\varepsilon - 7.888\varepsilon^2 \quad \text{for } \varepsilon > 0, \quad (7)$$

$$P_{pz}(GaN) = -0.918\varepsilon + 9.541\varepsilon^2 \quad (8)$$

The discussed basal strain function is

$$\varepsilon(x) = [a_{subs} - a(x)]/a(x), \quad (9)$$

In the case of pseudomorphic growth, basal strain e can be calculated directly from the lattice constants, which are found to follow Vegard's law as a function of composition:

$$a_{Al_xGa_{1-x}N} = 0.31986 - 0.00891x \quad (10)$$

Then the net polarization charge at the $Al_xGa_{1-x}N/Al_yGa_{1-y}N$ heterointerface is

$$\sigma_{Al_xGa_{1-x}N/Al_yGa_{1-y}N} = \left(P^{sp}_{Al_yGa_{1-y}N} + P^{pz}_{Al_yGa_{1-y}N}\right) - \left(P^{sp}_{Al_xGa_{1-x}N} + P^{pz}_{Al_xGa_{1-x}N}\right) \quad (11)$$

where $a(x)$ and a_{subs} are the lattice constants of the unstrained alloy at composition x, and of the substrate (assumed to be noncompliant), respectively. Other detailed material parameters of semiconductors used in this simulation can be found in Ref. 16.

RESULTS AND DISCUSSION

Figure 2 shows the light output power and IQE as a function of the injection current for the three samples. From Fig. 2a, it can be seen that there is little difference between three samples at low injection currents (0–20 mA). As the injection current further increases, the difference between the three samples increases (20–180 mA). When the conventional EBL of original LED is replaced by the trapezoidal EBL, the output power is enhanced obviously. Sample B with double trapezoidal EBLs possesses the highest output power. It is worth noting that the output powers of the three samples increase linearly as the forward current increases to 180 mA. When the injection current is 180 mA, the values of output power of original LED, sample A and sample B are 73 mW, 78 mW and 90 mW, respectively. Figure 2b plotted the IQE of three samples at the same current. It is evident that the IQE of sample A and B are higher than that of the original LED. At the peak value position, the maximum IQE of the original LED is 36.7%, while sample A and B are 40.1% and 44.1%. On the other hand, the efficiency drops of three samples are 8.3%, 7.2% and 4.6%, respectively. All these data indicate that the optical performance of sample B is the optimal among three samples.

In order to explain the reasons for the improvement of optical performance, these three structures are investigated by APSYS simulation to compare the electrostatic fields, energy band diagrams and carrier distributions as functions of the injection current. Figure 3 plots the energy band diagrams and the electron current densities of these three samples. As depicted in Fig. 3a, we can see that there is a clearly band downward sloped at the last barrier and EBL, it brings about that electrons overflow from the active region to the p-side layer and makes holes more difficult to inject into MQWs. In comparison, the downward band-bending of sample A and sample B become much smoother due to the decrease of electrostatic field at last quantum barrier (LQB)/EBL interface (shown in Fig. 4b). Figure 3a shows that the effective electron and hole barrier height of original LED are 262.5 meV and 270.4 meV. Additionally, when the

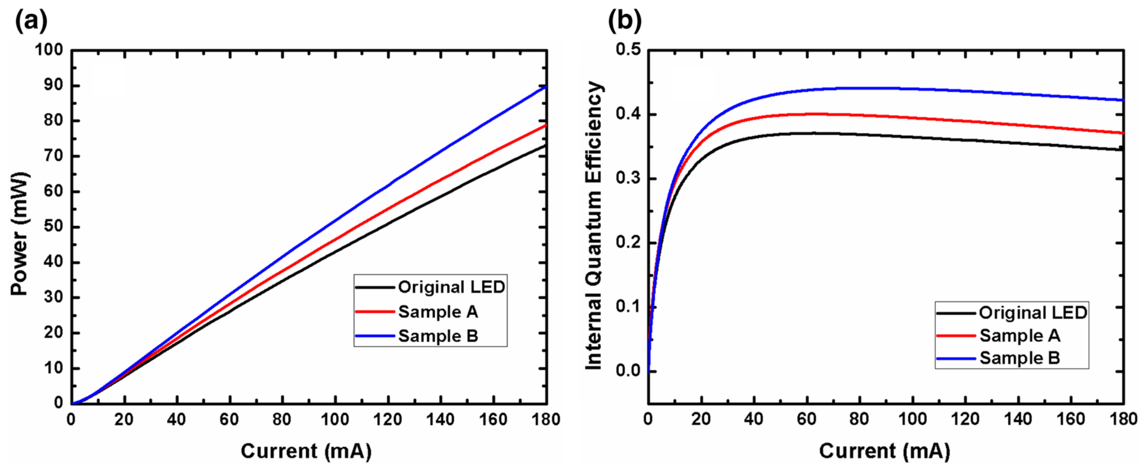

Fig. 2. (a) The light output power and (b) internal quantum efficiency as a function of current for the three samples.

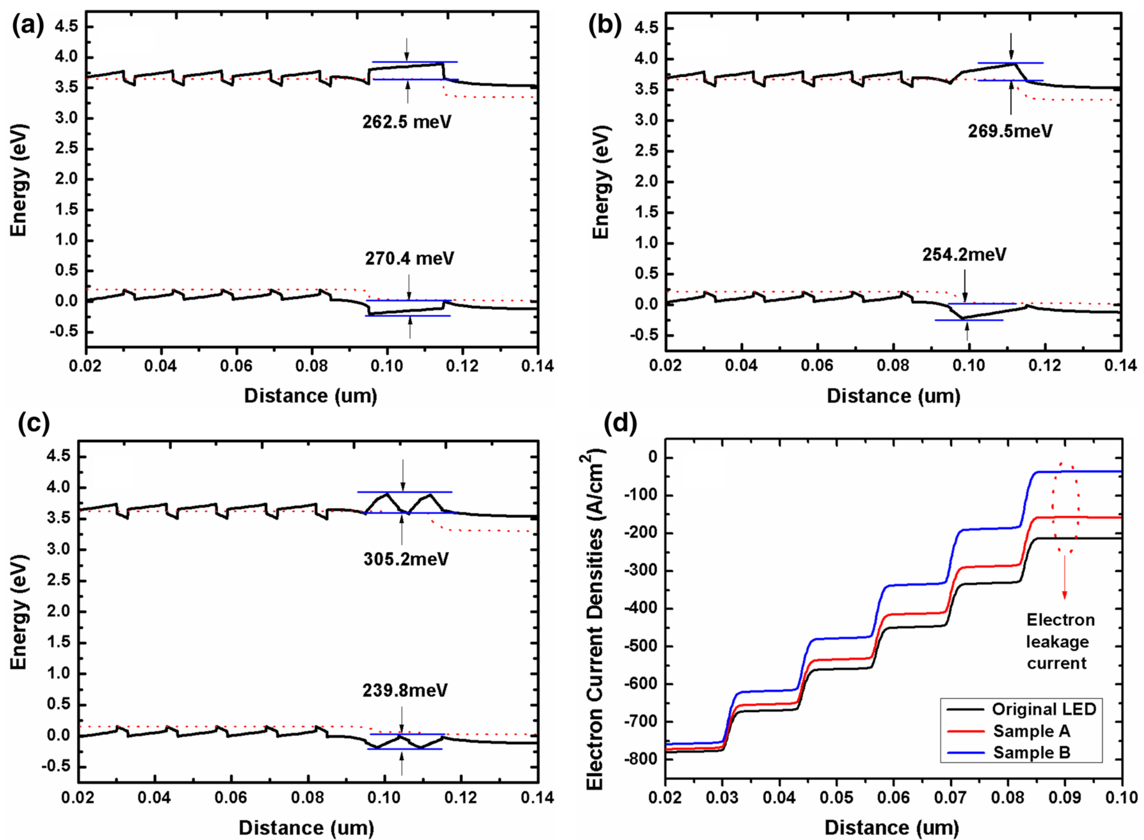

Fig. 3. Energy band diagrams of (a) original LED, (b) Sample A, (c) Sample B and the electron current density diagram (d) for the three samples at 180 mA.

traditional EBL is replaced by the trapezoidal EBL as shown in Fig. 3b and c, the barrier effective height for electron is increased from 269.5 meV (sample A) to 305.2 meV (sample B) and the height for hole is fall from 254.2 meV (sample A) to 239.8 meV (sample B). Obviously, sample B has higher effective electron barrier height and lower effective hole barrier height than the other two samples. This means that the specially designed trapezoidal EBL can efficiently reduce the leakage of electron and improve the injection of hole. The electron current densities of the three samples are plotted in Fig. 3d. In sample B, the electron current density in *p*-type side is 32 A/cm^2, which is much smaller than that of sample A (157 A/cm^2) and original LED (212 A/cm^2). As previously shown,[17] the electron overflow from the active region into the *p*-type region is viewed as leakage current.

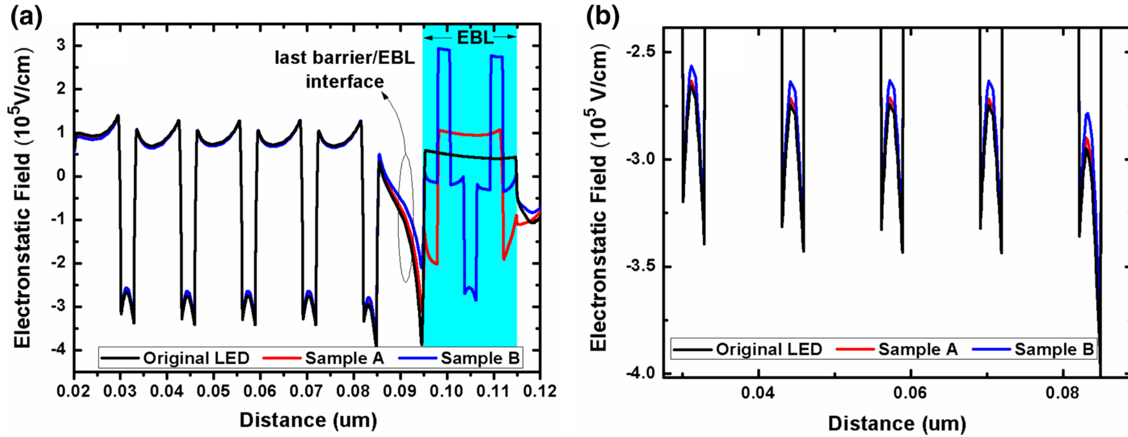

Fig. 4. (a) The electrostatic field around the EBL for the three samples and (b) enlarged electrostatic field in the active region for the three samples at 180 mA.

Therefore, the electron leakage current is severe in original LED, and it obviously decreases in sample B. So in sample B with double trapezoidal EBL, just a small amount of electrons escape out of active region, and most of the electrons contribute to radiative recombination, which leads to high output power and internal quantum efficiency. According to the above data, it can be found that when the current is injected at both ends of the LED, sample B with double trapezoidal EBL can effectively increase the capability of electron restriction and enhance the hole injection efficiency in MQWs compared with sample A and original LED, thereby increasing the radiative recombination rate.

Figure 4 presents the electrostatic field of the three devices and the detailed view at the (LQB)/EBL interface. As shown in Fig. 4a, it is evident that the original LED possesses a much stronger electrostatic field in the LQB/EBL interface because of the high surface charge density. Because of the smaller electrostatic fields, the situations of downward band-bending at the interfaces near the EBL of two redesigned structures are slighter than that of the original one, which is not only enlarging the spatial overlap of electron and hole wave functions, but also enhancing the hole injection efficiency and suppressing the electron leakage, which coincides with the result of Ref. 10. Large electrostatic field in EBL region will increase the band edge of the electron blocking layer, which will contribute to electron leakage suppression. Therefore, compared with the other two structures, sample B can suppress electron leakage more effectively. Figure 4b shows enlarged electrostatic field of three samples in the active region. The electrostatic field in the active region of sample B is smallest, which can reduce quantum-confined Stark effect and improve the radiative recombination rate in active region. Thus, sample B has an advantage over the other two samples in radiative recombination.

Figure 5 shows the distribution of electron and hole concentrations in the three structures. Note that the horizontal positions of samples A and B in Fig. 5 are shifted slightly for better observation. According to Fig. 5a, it can be seen that electron concentration of sample A does not change significantly compared with the original LED. However, the electron concentration of sample B in the MQW region is larger than that of original LED and sample A. At the same time, the hole concentration in the active region is also increased apparently from original LED to sample B, which is plotted in Fig. 5b. In addition, it's clear that the electron concentration around the LQB/EBL interface of sample B is the lowest among three samples, which indicates sample B has better electron blocking capability compared with the original LED and sample A. Moreover, it is worth noting that the hole concentration around the top of the EBL of sample B is the lowest, which illustrates sample B possesses the best hole injection efficiency. The improvement of electron concentration in MQWs is due to the use of the double trapezoidal EBL, which enhances the capability of electron confinement in UV-LED. Because we adopted the trapezoidal EBL structure, the effective barriers of hole in the valence band become lower, thereby the hole concentration in the active area of the UV-LED is increased.

In order to make sure the double trapezoidal EBL contributes to light emission, the radiative recombination rates and spontaneous emission rates in three samples are researched, which are shown in Fig. 6. According to the analysis above, with the reduction of electron leakage and the enhancement of hole injection, more carriers in active region contribute to the radiative recombination. As a result, the radiative recombination rate in sample B is higher than that of the other two samples, which is plotted in Fig. 6a. The spontaneous emission rates of the three samples are shown in Fig. 6b. It is worth noting that the peak wavelength of the three samples are the same and it is about 352 nm, illustrating that the optimized structures does not change the emission wavelength of the UV-LED. In

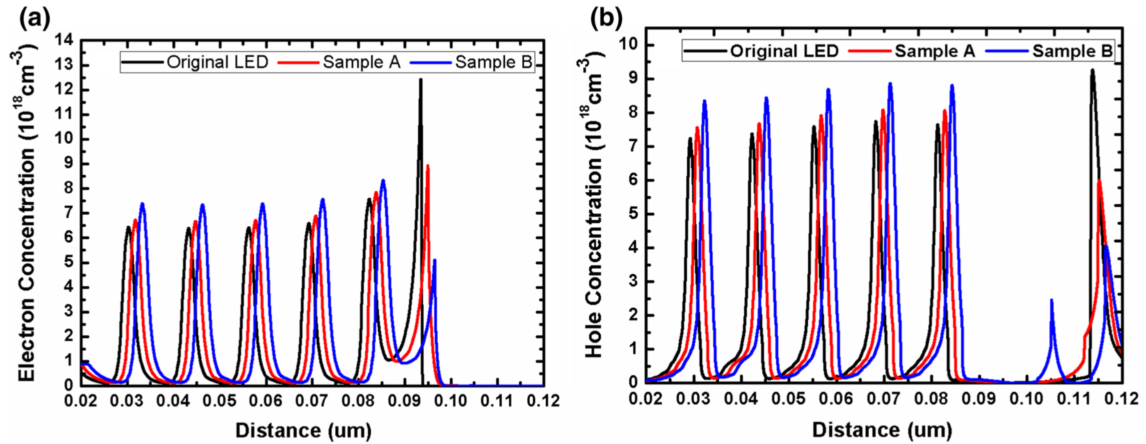

Fig. 5. (a) Electron concentration (b) Hole concentration distribution within MQWs and near the EBL area of the three samples at 180 mA.

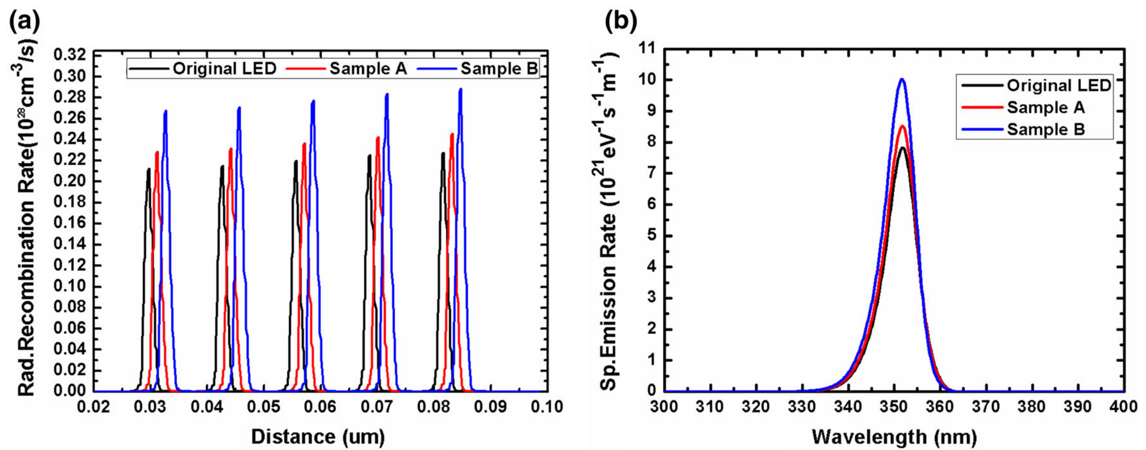

Fig. 6. (a) Radiative recombination rates distribution and (b) spontaneous emission spectrum for the three samples at 180 mA.

addition, it can be seen that the spontaneous emission spectrum peak of sample B is significantly stronger than that of original LED and sample A, which results from its enhanced radiative recombination rate.

According to a series of analysis about the physical properties of the three samples, it is believed that the application of the trapezoidal EBL prompts the enhancement of effective potential barriers of electron and the fall of effective potential barriers of hole. These cause more electrons and holes to exist and accumulate in the active region of sample B, which contributes to the radiative recombination directly. Consequently, the performance of sample B is better than that of the other two samples.

CONCLUSIONS

In summary, we have investigated the performance of AlGaN-based UV-LEDs with trapezoidal EBL. The output power, IQE, energy band, carrier concentration and radiative recombination have been simulated by APSYS software. The results show that the trapezoidal EBL of optimized samples play a significant role in affecting electron leakage and hole injection efficiency. The optimized structure can not only alleviate the polarization fields between the active region and EBL, but also cause the decrease of potential height for hole and the increase of potential height for electron, which led to higher radiative recombination rates. The electron leakage current markedly reduces. Furthermore, the efficiency droop of the optimized structure also improves. So the UV-LEDs with trapezoidal EBL can significantly improve optical and electrical performance.

ACKNOWLEDGMENTS

This project was supported by National Natural Science Foundation of China National Key Scientific Research Instrument Development Project, China (Grant No. 61527825), Natural Science Foundation of Guangdong Province,China (Grant No. 2015A030313370).

REFERENCES

1. A. Khan, K. Balakrishnan, and T. Katona, *Nat. Photonics* 2, 77 (2008).

2. R. Gaska, C. Chen, J. Yang, E. Kuokstis, A. Khan, G. Tamulaitis, I. Yilmaz, M.S. Shur, J.C. Rojo, and L.J. Schowalter, *Appl. Phys. Lett.* 81, 4658 (2002).
3. J. Li, J.Y. Lin, and H.X. Jiang, *Appl. Phys. Lett.* 88, 171909 (2006).
4. T. Böttcher, S. Figge, S. Einfeldt, R. Chierchia, R. Kröger, and C. Petter, *Phys. Status Solidi* 5, 1846 (2010).
5. K. Kazlauskas, A. Žukauskas, G. Tamulaitis, J. Mickevičius, M.S. Shur, R.S. Qhalid Fareed, J.P. Zhang, and R. Gaska, *Appl. Phys. Lett*. 87, 172102 (2005).
6. L. Gao, *Opt. Quantum Electron.* 47, 1 (2014).
7. Y. Zhang, S. Gautier, C.Y. Cho, E. Cicek, Z. Vashaei, R. Mcclintock, C. Bayram, Y. Bai, and M. Razeghi, *Appl. Phys. Lett*. 102, 011106 (2013).
8. L. Zhang, K. Ding, N.X. Liu, T.B. Wei, X.L. Ji, P. Ma, J.C. Yan, J.X. Wang, Y.P. Zeng, and J.M. Li, *Appl. Phys. Lett.* 98, 062103 (2011).
9. C. Liu, Z.W. Ren, X. Chen, B.J. Zhao, and X.F. Wang, Shuti Li. *IEEE Photonics Technol. Lett.* 26, 1368 (2014).
10. G. Li, W.D. Song, H. Wang, X.J. Luo, X. Luo, and S.T. Li, *IEEE Photonics Technol. Lett*. 30, 1071 (2018).
11. S.H. Yen, M.C. Tsai, M.L. Tsai, Y.J. Shen, T.C. Hsu, and Y.K. Kuo, *IEEE Photonics Technol. Lett.* 21, 975 (2009).
12. Y.K. Kuo, M.C. Tsai, S.H. Yen, T.C. Hsu, and Y.J. Shen, *IEEE J. Quantum Electron.* 46, 1214 (2010).
13. S.H. Yen and Y.K. Kuo, *J. Appl. Phys.* 103, 071121 (2008).
14. W. Tian, Z.H. Feng, B. Liu, H. Xiong, J.B. Zhang, J.N. Dai, S.J. Cai, and C.Q. Chen, *Opt. Quantum Electron.* 45, 381 (2013).
15. V. Fiorentini, F. Bernardini, and O. Ambacher, *Appl. Phys. Lett.* 80, 1204 (2002).
16. I. Vurgaftman, J.R. Meyer, and L.R. Ram-Mohan, *J. Appl. Phys.* 89, 5815 (2001).
17. K. Suzue, S.N. Mohammad, Z.F. Fan, W. Kim, O. Aktas, A.E. Botchkarev, and H. Morkoç, *J. Appl. Phys.* 80, 4467 (1996).

Publisher's Note Springer Nature remains neutral with regard to jurisdictional claims in published maps and institutional affiliations.